REVIEW

Active Sites for Adsorption and Reaction of Molecules on Rutile TiO_2(110) and Anatase TiO_2(001) Surfaces†

Shi-jing Tan, Bing Wang*

Hefei National Laboratory for Physical Sciences at the Microscale and Synergetic Innovation Center of Quantum Information and Quantum Physics, University of Science and Technology of China, Hefei 230026, China

(Dated: Received on June 18, 2015; Accepted on July 5, 2015)

The reactivity of specific sites on rutile TiO_2(110)-(1×1) surface and anatase TiO_2(001)-(1×4) surface has been comparably studied by means of high resolution scanning tunneling microscopy. At the rutile TiO_2(110)-(1×1) surface, we find the defects of oxygen vacancy provide distinct reactivity for O_2 and CO_2 adsorption, while the terminal fivefold-coordinated Ti sites dominate the photocatalytic reactivity for H_2O and CH_3OH dissociation. At the anatase TiO_2(001)-(1×4) surface, the sixfold-coordinated terminal Ti sites at the oxidized surface seem to be inert in both O_2 and H_2O reactions, but the Ti-rich defects which introduce the Ti^{3+} state into the reduced surface are found to provide high reactivity for the reactions of O_2 and H_2O. By comparing the reactions on both rutile and anatase surfaces under similar experimental conditions, we find the reactivity of anatase TiO_2(001) is actually lower than rutile TiO_2(110), which challenges the conventional knowledge that the anatase (001) is the most reactive TiO_2 surface. Our findings could provide atomic level insights into the mechanisms of TiO_2 based catalytic and photocatalytic chemical reactions.

Key words: TiO_2, Rutile, Anatase, Photocatalysis, Scanning tunneling microscopy

I. INTRODUCTION

TiO_2 has been studied extensively for its potential applications in solar energy conversion, clean hydrogen energy, and environmental remediation [1–10]. Among the three different phases of TiO_2, rutile is recognized as the most stable phase [11], and its (110) surface serves as a model oxide surface in the fundamental studies of catalytic reactions [2–4]. Numerous efforts had been made on the rutile TiO_2(110) surface, but some fundamental issues still need to be clarified. For instance, it has long been debated whether the initial reaction step of H_2O molecules can undergo oxidation by photogenerated holes on rutile TiO_2(110) surface [5, 12–14]. The anatase phase of TiO_2 is widely concerned for its high reactivity [7, 15, 16] and a common perception is that the anatase phase is inherently more photoactive than the rutile phase [8]. Also, many theoretical works predicted that the (001) surface should be the most reactive among the different facets of anatase TiO_2 [17–19], but the structural properties of the perfect surface as well as the possibly existed defects on the (001) surface have not been well examined experimentally.

Recently we have systematically studied these two surfaces by using scanning tunneling microscopy (STM), joint with spectroscopic method and theoretical calculations [20–30]. STM provides an ideal tool to characterize the surface structures and defects, and thus could give insights into the atomic level understanding of the reactivity of TiO_2 surface [2, 4]. Various molecules, like O_2, CO_2, H_2O and CH_3OH, have been used to detect the activity of the two surfaces and to identify specific active sites. Here, we summarize our recent studies about the adsorption and reaction behaviors of these molecules on the rutile TiO_2(110)-(1×1) surface and anatase TiO_2(001)-(1×4) surface.

II. ADSORPTION AND REACTION OF MOLECULES AT OXYGEN VACANCIES ON RUTILE TiO_2(110)-(1×1) SURFACE

The rutile TiO_2(110) is a prototypical oxide surface in the studies of catalytic and photocatalytic chemical reactions [2–4, 6]. Under Ar^+ ion sputtering and ultrahigh vacuum (UHV) annealing, the single-crystal TiO_2(110) can be reduced accompanying with the generation of defects, such as Ti interstitials in subsurface [31, 32] and oxygen vacancies (O_V) at surface [20, 33–35]. The reduced TiO_2(110)-(1×1) surface consists of alternated rows of fivefold-coordinate Ti rows (Ti_{5c}) and twofold-coordinate bridging oxygen rows (O_{br}) along the [001] direction, as schematically shown by the ball-and-stick model in Fig.1(a). Although the

†Dedicated to Professor Qing-shi Zhu on the occasion of his 70th birthday.

*Author to whom correspondence should be addressed. E-mail: bwang@ustc.edu.cn

Ti_{5c} rows are geometrically lower than the O_{br} rows, in the typical empty-state STM images the contrast of Ti_{5c} rows are much brighter than the O_{br} rows, as shown in Fig.1(b), which is because the unoccupied Ti 3d dominates the electron states in the empty state STM image [36]. The bright spots in the O_{br} rows in the STM image (Fig.1(b)) are the defects of O_V, which have a typical concentration in the range from 0.04 to 0.22 monolayer (1 monolayer=5.2×10^{14} cm^{-2}) in our experiments.

Each O_V defect could introduce two excess electrons to the surface, and these electrons partially fill into the unoccupied 3d orbital of the neighboring Ti atoms and form a defect state in the band gap at about 0.9 eV below the Fermi level [35, 37–39]. The occupied state STM images at a negative bias voltage were obtained to characterize the spatial distribution of the electrons of O_V. Figure 1(c) is the empty-state STM image of an O_V defect, and its occupied state image (Fig.1(d)) shows a symmetric four-lobed shape along the Ti_{5c} rows in the vicinity of the O_V defect and each lobe extends over several Ti_{5c} sites. The appearance of O_V in the occupied state image is quite different from the empty state image. Such appearance suggests the excess electrons of O_V are delocalized and even spread over more than 10 Ti_{5c} sites. Density functional theory (DFT) calculations were performed to obtain the geometric and electronic structures of the O_V. A (10×1) supercell with one missing bridging-oxygen was used to simulate the O_V with an O_V concentration of 0.1 monolayer. The simulated empty and occupied state STM images of O_V are shown in Fig.1 (e) and (f), respectively, which support the experimental observations very well. The delocalized character of defect electrons should also be reflected by the adsorption and reaction behaviors of molecules [40–44].

To address this, we studied the adsorption and dissociation of O_2 and CO_2 molecules at O_V. Molecular O_2 is recognized as a typical electron scavenger [38], which can assist the charge separation in TiO_2 [45]. The generated O_2^{2-}, $O_2^{\cdot-}$, O^- and *etc.* will act as active species in the oxidation reactions of CO and organic pollutants [7]. The chemistry of O_2 on TiO_2(110)-(1×1) surface has been studied by numerous experimental methods and theoretical calculations [46–56]. The O_V defects provide the main specific sites for O_2 adsorption and dissociation on TiO_2(110) surface. Henderson *et al.* reported up to three O_2 molecules could adsorb per O_V defect. Upon heating, one O_2 dissociates to heal the O_V site and the other two desorb from the surface at 410 K [57]. Kimmel *et al.* confirmed that two O_2 molecules could chemisorb per O_V and convert to a stable tetraoxygen as annealed above 200 K by the methods of temperature programmed desorption (TPD) and electron-simulated desorption [47]. Although the molecular state O_2 at O_V had been confirmed widely for a long time, it was not observed by STM until 2010 [24, 58, 59].

In our study by using the *in situ* STM method, we

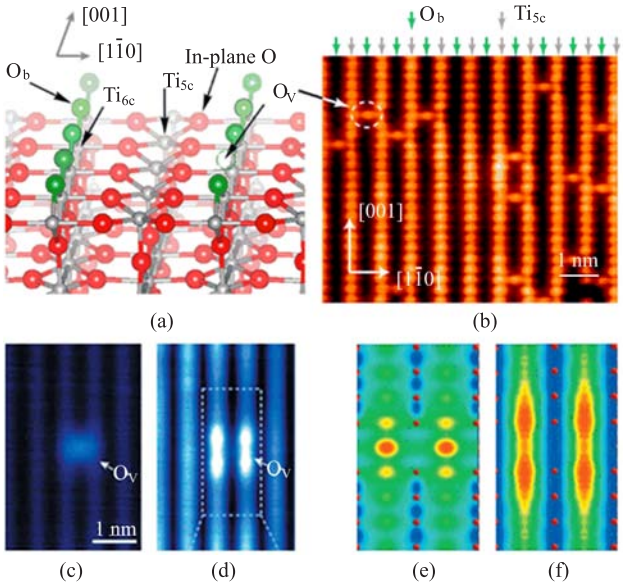

FIG. 1 (a) The ball-and-stick model of the reduced TiO_2(110)-(1×1) surface. (b) An atomic resolved empty state STM image of the reduced TiO_2(110)-(1×1) surface, imaged at 1.0 V and 10 pA. (c) and (d) The empty state (1.4 V, 10 pA) and occupied state (−1.4 V, 5 pA) STM images of an O_V defect. (e) and (f) Theoretical simulation of the empty state (1.0 V) and occupied state (−1.1 V) STM images of O_V respectively. (c)−(f) Modified with permission from Ref.[36], copyright 2009 American Institute of Physics.

observe the chemisorbed molecular O_2 at O_V, which has a very faint contrast in STM image and is easily to be dissociated by tunneling electrons [24]. Figures 2 (a) and (b) are the same area images before and after 0.04 Langmuir O_2 dosing to the surface. It is observed several O_V defects (yellow rectangles in Fig.2(a)) change to misty characters (white rectangles in Fig.2(b)) after O_2 dosing, indicating singly adsorbed O_2 molecules at O_V. Such misty characters of O_2 at O_V is consistent with the observation by Scheiber *et al.* [58] and Wang *et al.* [59]. Optimized structure of O_2 at O_V in Fig.2(c) shows a flat-lying structure with the O−O bond perpendicular to the O_{br} row. The simulated STM image of O_2 at O_V in Fig.2(d) shows a faint appearance, which is in good agreement with the experimental observations. The calculated O−O bond length is about 1.44 Å, which is close to the 1.46 Å O−O distance in H_2O_2, suggesting that the molecular O_2 at O_V should be doubly charged as a peroxide O_2^{2-}. Charge density difference calculations in Fig.2(e) suggest the excess electrons of O_V will symmetrically accumulate to the O atoms of the peroxide O_2^{2-}.

Figure 2(f) schematically shows a flat-lying molecular O_2 at O_V and the STM image was imaged at a low bias of 0.6 V to reduce the destructivity of the tunneling electrons. When the molecular O_2 at O_V was imaged at a higher bias voltage, say 1.0 V, the O_2 can be excited to an intermediate state. Such intermediate state was

DOI:10.1063/1674-0068/28/cjcp1506129

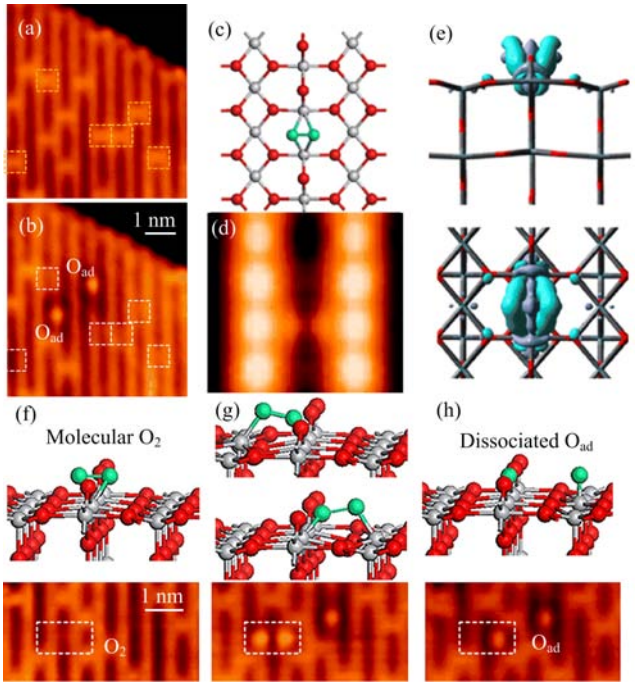

FIG. 2 (a,b) Same area STM images obtained before and after O_2 dosing to TiO_2(110)-(1×1) surface. Yellow rectangles: original O_V sites, white rectangles: singly adsorbed O_2 at O_V. Imaged at 1.0 V and 10 pA. (c) Optimized structure of O_2 at O_V. (d) Simulated STM image of O_2 at O_V, showing a very faint appearance. (e) Side (upper) and top views (lower) of the charge density difference of O_2 at O_V. (f) Schematic drawing of molecular O_2, the STM image is obtained at 0.6 V, 10 pA. (g) The intermediate state of O_2 excited by the tunneling electrons. (h) The dissociated state of O_2, with one O atom healing the O_V and the other O bonding to the adjacent O_b. Modified with permission from Ref.[24], copyright 2011 American Chemical Society.

imaged as the paired protrusions at opposite Ti_{5c} sites near the O_V defect as shown in Fig.2(g) (marked by the rectangle). On the basis of DFT calculations, such intermediate state is suggested to result from the fast switching between the inclined configuration (models in Fig.2(g)) and the flat-lying (model in Fig.2(f)) configurations of O_2 at O_V, which is excited by the inelastic tunneling electron. The switching behavior of O_2 at O_V was further detected by current-time (I-t) curve measurements at 5.2 K and the switching rate was found to increase dramatically at the higher bias voltages and elevated temperatures. The intermediate state O_2 will finally dissociate with one O atom filling into the O_V and the other O forming an adatom (O_{ad}) at the near Ti_{5c} site (Fig.2(h)). The dissociated O_{ad} can also be observed in Fig.2(b) after O_2 adsorption.

At higher coverage after all the O_V defects are fully filled, the O_2 can also adsorb at Ti_{5c} sites. We find the O_2 at Ti_{5c} is very easy to be dissociate by STM tip, forming a pair of O_{ad}. Wang *et al.* observed the molecular O_2 appeared at Ti_{5c} as a single protrusion at 50 K by using an "extremely mild" tunneling parameters of 0.3 V and 1 pA. They also found the O_2 could be dissociated by STM tip or at elevated temperature [59]. In addition to such tip-induced O_2 dissociation at Ti_{5c} sites at low temperature, Wendt *et al.* proposed a mechanism that the Ti interstitials in the near-surface region might be largely responsible for the O_2 dissociation at Ti_{5c} sites [32]. Later, Du *et al.* claimed that the itinerant electrons associated with the O_V were being utilized in the O_2 dissociation at the Ti_{5c} sites [60].

In our study, we have further concerned the role of O_2 in CO oxidation [25, 26, 29]. It is found the dissociated O_{ad} has no activity for low temperature CO oxidation and the interaction between CO and O_{ad} could only form CO-O or CO-O-CO complexes [25]. Instead, the molecular O_2 at O_V is proposed to be responsible for CO oxidation under a photo excitation in our recent first principle study [29]. The calculation suggests at the ground state, the O_2 molecule prefers to be adsorbed at the O_V horizontally. Under photo excitation, the ground state O_2 could capture a hole as it transforms itself into a near-perpendicular geometry. Such a photo-excited O_2 could be effectively connected to the CO molecule to form an O-O-CO complex and capture an electron, which could then convert to CO_2 by overcoming a very small barrier. The whole process implies that both hole mediated and electron mediated steps are necessary for the complete CO photo-oxidation reaction by molecular O_2 [29]. Interestingly, similar multiple steps in photo-oxidization of CO by O_2 were later reported by Petrik and Kimmel studied by the photon-stimulated desorption at a millisecond time scale [61].

CO_2 reduction is one of the primary steps in the artificial photosynthesis [62–70]. The study of CO_2 on rutile TiO_2(110) surface by STM can provide meaningful information, such as the adsorption, diffusion and reaction behaviors [71–75]. In our study, the single electron attachment is confirmed to be responsible for CO_2 dissociation and the dependence of CO_2 dissociation on the energy of the injected electrons is accurately measured (Fig.3(a)) [23]. It is found that CO_2 dominantly adsorbs at O_V defects at low CO_2 coverages, and may occur at Ti_{5c} at higher coverage when the O_V defects have been fully filled. Figure 3 (b) and (c) are the images acquired within the same area before and after CO_2 dosing at 80 K. The brighter spots emerged at the original O_V sites are the singly adsorbed CO_2. It is found that CO_2 may occur at Ti_{5c} sites, but is still diffusive even at a much lower temperature of 15 K. Our DFT calculations suggest a linear configuration (both vertical and inclined) of CO_2 adsorption at the O_V. Charge density difference calculations confirm the net charge transfer between the CO_2 and the O_V is small, which implies the CO_2 almost keeps neutral at O_V defect. After high voltage pulses were applied to the CO_2 molecule marked by "×" in Fig.3(c), the CO_2 disappeared and also the original O_V defects were healed (Fig.3(d)). The results indicate the CO_2 dissociates with the lower C−O

DOI:10.1063/1674-0068/28/cjcp1506129

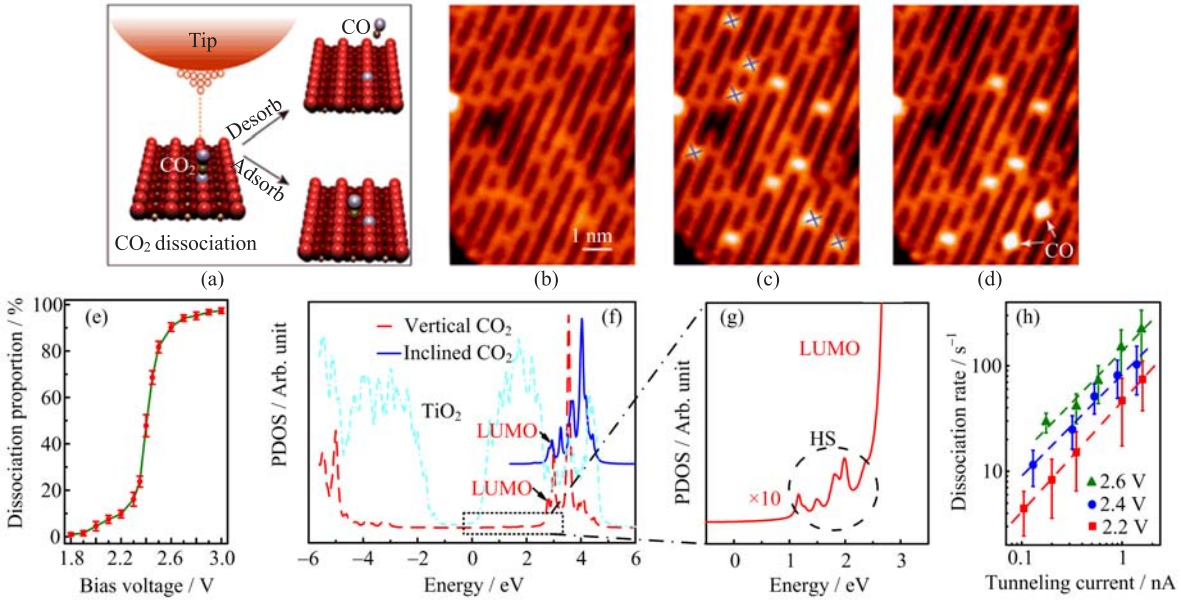

FIG. 3 (a) Schematic drawing of the tip-induced CO_2 dissociation at O_V on TiO_2(110)-(1×1) surface. The produced CO might either desorb or adsorb at a near Ti_{5c} site. (b) and (c) Same area STM images before and after CO_2 dosing. The symbols of "×" mark the point pulse positions. (d) STM image obtained after the point pulses were applied. STM images are obtained at 1.0 V and 10 pA at 80 K. (e) Dissociation fraction of CO_2 measured as a function of the applied bias voltage. (f) Calculated PDOS of the vertical and inclined CO_2 at O_V. The PDOS is shifted from each other for clarity. (g) The magnified PDOS of the weak hybridization states below LUMO. (h) Log-log plot of CO_2 dissociation rate as a function of the tunneling current measured at different bias voltages. The linear fitted slop is 0.98±0.10 (2.6 V), 0.96±0.07 (2.4 V) and 1.05±0.01 (2.2 V). Modified with permission from Ref.[23], copyright 2011 American Physical Society.

bond breaking. The produced CO may escape to vacuum and some may re-adsorb at the near Ti_{5c} sites as marked by the arrows in Fig.3(d). We obtained a threshold voltage of 1.8 V for CO_2 dissociation and a rapid dissociation region around 2.3 V, as shown in Fig.3(e). Our DFT calculations give the partial density of states (PDOS) in Fig.3 (f) and (g), in which the lowest unoccupied molecular orbital (LUMO) of CO_2 locates at 2.3 eV above the TiO_2 conduction band onset and strongly hybridizes with the Ti 3d orbital of the O_V. According to the experimental measurement, we propose that the LUMO of CO_2 dominates the electron injection channel and the hybridization states are responsible for the threshold voltage for CO_2 dissociation. We further measured the dissociation rate (R_d) as a function of the tunneling current (I) at different voltages of 2.6, 2.4, and 2.2 V (Fig.3(h)). According to the relation of $R_d \propto I^N$, the fitted values of N are 0.98±0.10, 0.96±0.07, and 1.05±0.01 at 2.6, 2.4, and 2.2 V respectively, which clearly imply the dissociation process involves only one electron per CO_2 dissociation event.

Our results suggest that a single electron could attach to the neutral CO_2 molecule at O_V through its LUMO or unoccupied hybridization states, forming a $CO_2^{\cdot-}$. The energy of 2.3 eV, at which the fast CO_2 dissociation takes place, may reflect the reduction potential of the $CO_2^{\cdot-}/CO_2$ couple at TiO_2 surface. The activated $CO_2^{\cdot-}$ will then dissociate to a CO, leaving an O atom heals the O_V. Such electron attachment induced CO_2 dissociation at TiO_2(110) was also well obtained by Acharya *et al.* [71] and Lee *et al.* [73].

Furthermore, we find the CO_2 at O_V cannot be photocatalytically dissociated by irradiation with a 266 nm laser. This may be due to the quick thermalization of the photogenerated electrons to conduction band (CB) minimum [8, 76], which is much lower than CO_2 LUMO and the hybridization states. The large energy mismatch thus prevents the electron transfer from TiO_2 substrate to CO_2. One of possible way is to use TiO_2-CuO cocatalyst, where the CuO CB minimum is higher than the CO/CO_2 potential and helps the transfer of the photogenerated electron to the CO_2 molecules [69].

III. ADSORPTION AND REACTION OF MOLECULES AT Ti_{5c} SITES ON RUTILE TiO_2(110)-(1×1) SURFACE

The water splitting reaction based on the prototypical TiO_2 photocatalyst is one of the fundamental processes that bears significant implications in solar energy conversion, hydrogen energy technology and artificial photosynthesis [5, 12–14, 28, 77]. By introducing the UV light to STM scanning area, we can directly observe how a single H_2O molecule could be dissociated by the UV light. The initial dissociation step of $h^+ + H_2O \rightarrow \cdot OH + H^+$ by photo generated holes has been

DOI:10.1063/1674-0068/28/cjcp1506129

revealed [22], where h^+ denotes the hole.

We first studied the adsorption behavior of H_2O at TiO_2(110)-(1×1) surface. From TPD studies, it is known that H_2O may adsorb both at the Ti_{5c} sites and at O_V sites, but with different desorption temperatures of about 265 and 490 K, respectively [78–80]. Figure 4 (a) and (b) show the images before and after H_2O dosing at 80 K. The bright round spots are singly adsorbed H_2O molecules at Ti_{5c} sites and the spot marked by the white arrow is a H_2O molecule at O_V defect. It has been pointed out that H_2O adsorbed at O_V can dissociate to two hydroxyl groups (OH_b) at elevated temperatures [81, 82]. We find that H_2O at O_V can keep molecular form at 80 K (Fig.4(c)), and can be dissociated to an OH_b pair at higher bias voltages. As shown in Fig.4(d) the spot expands to two lattice sites after scanning at 2.0 V, which indicates the H_2O molecule dissociates to a pair of OH_b. Such dissociation for H_2O at O_V is mainly thermal-activated or tip-induced process. Differently, the H_2O molecules adsorbed at Ti_{5c} sites are quite stable against relatively high bias voltages [22]. At 80 K, H_2O at Ti_{5c} is almost immobile, but at elevated temperatures, H_2O could diffuse along Ti_{5c} rows to form water dimer [83] and H_2O chains [84]. Several work suggested the molecular and dissociative H_2O at Ti_{5c} had almost equivalent energies [85, 86], which implied that the molecular and the dissociative H_2O may occurs simultaneously at Ti_{5c}, but no STM result has been observed.

As shown in Fig.4(e), when a 2.4 V pulse was applied to the lower-left H_2O molecule, it changed to a fuzzy spot which was assigned as a hydroxyl group at Ti_{5c} site (OH_t). Another 2.4 V pulse could further dissociate the OH_t to an O_{ad}. A higher voltage pulse of 2.8 V could directly dissociate the upper-right H_2O to an O_{ad}, with removal of both the two H atoms. Such tunneling electron induced stepwise H_2O dissociation processes are modeled in Fig.4(f), which might follow a similar mechanism as H desorption from OH_b group by voltage pulse [81, 87].

The photocatalytic dissociation of H_2O was further studied by introducing the UV light to the STM. The images before and after light irradiation were always compared to trace any reaction event. We have performed the experiments under light irradiation with different wavelengths from different light sources, such as mercury-xenon lamp with bandpass filters (400±40 and 440±20 nm), Nd:YAG laser (532, 355, and 266 nm), excimer laser (193 nm). A specially coated sapphire window (VG Scienta) was employed for 193 nm UV light with 90% transmission. During the light irradiation, the tip was retraced back for about 10 μm, which could avoid the shadowing effect. The temperature fluctuation was less than 2 K during light irradiation and the thermal drift was less than 10 nm/h at about 80 K, which allowed us to always get back to the same areas after light irradiation.

Figure 5 (a) and (b) show a set of *in situ* experiments

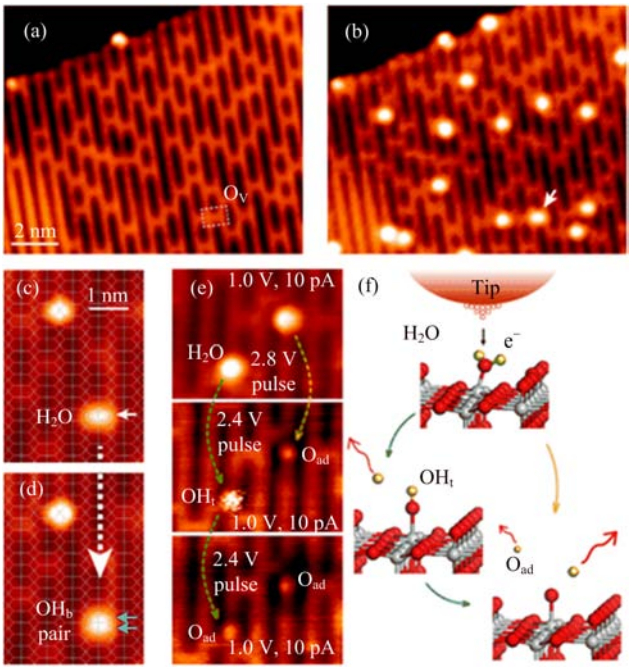

FIG. 4 (a, b) Same area STM images of TiO_2(110)-(1×1) surface before and after H_2O adsorption at 80 K. (c, d) Images obtained before and after a 2.0 V scanning. White arrow: H_2O at O_V defect, blue arrows: a pair of OH_b groups. (e) Tunneling electron induced stepwise dissociation of H_2O at Ti_{5c} sites. (f) Structural models of the electron induced H_2O dissociation at a Ti_{5c} site. All the STM images are obtained at 1.0 V and 10 pA at 80 K. Modified with permission from Ref.[22], copyright 2012 American Chemical Society.

of UV induced H_2O dissociation. After the surface was illuminated by 400 nm light for 1 h two H_2O molecules disappear accompanying with two OH_b groups occurred at the adjacent O_b sites, respectively (Fig.5(b)). A fuzzy OH_t species appeared at a near Ti_{5c} site away from the original place by several lattice distances. The process is schematically shown in Fig.5 (c)−(f), where one of the H atoms transfers to the adjacent O_b site yielding an OH_b and the left OH either desorbed from surface as an ·OH (Fig.5(e)) or adsorbed at a near Ti_{5c} as an OH_t (Fig.5(f)).

We further checked the H_2O dissociation behavior under the light irradiation with different wavelengths. The H_2O could be dissociated under 193, 266, 355, and 400 nm light irradiation, but no dissociation event was observed under 440 and 532 nm light irradiation. The wavelength dependence well corresponds to the TiO_2 bandgap of 3.05 eV, where only the light with wavelength shorter than 400 nm can absorbed. Therefore, the observed H_2O dissociation could be attributed to the photocatalytic reaction. By comparing with the tunneling electron induced H_2O dissociation, we suggest the photocatalytic H_2O dissociation is dominated by photo-excited holes in valence band (Fig.5(g)). It should be mentioned that although we do observe the

DOI:10.1063/1674-0068/28/cjcp1506129

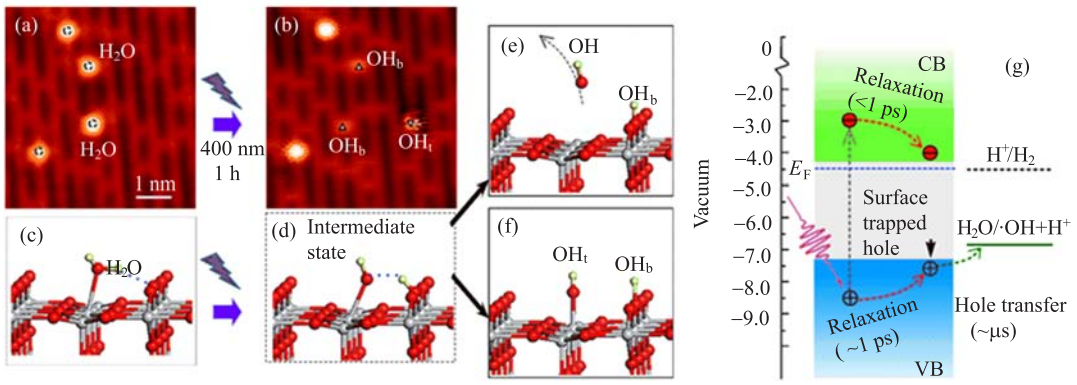

FIG. 5 (a) STM image of the individual H_2O molecules adsorbed $TiO_2(110)$-(1×1) surface. (b) The same area STM image after 1 h 400 nm light irradiation. Images are obtained at 1.0 V, 10 pA, and 80 K. (c)−(f) Structure models of photocatalytic H_2O dissociation at a Ti_{5c} site. (g) Energy diagram and relaxation time scales of the electron-hole pair excited by photon with energy larger than the TiO_2 bandgap. The redox potentials of $H_2O/\cdot OH$ and H^+/H_2 are shown to compare with the edges of valence band and conduction band of TiO_2. Modified with permission from Ref.[22], copyright 2012 American Chemical Society.

photocatalytic H_2O dissociation, the dissociation fraction is quite low, typically 2% and 4% after UV irradiation for 1 and 2 h respectively. The dissociation fraction cannot be increased by increasing the light intensity from 1.0−10 mW/cm^2. It seems even the low intensity of 1.0 mW/cm^2 used in our experiments is already saturated for H_2O dissociation. Although the underlying mechanism is not well understood yet, this behavior should be related to the "low intensity illumination" suggested by some previous work [13, 88–91].

A recent work by Lee *et al.* reproduced the electron induced H_2O dissociation process. They also found by using a negative bias voltage pulse to inject holes to H_2O molecule could lead to the formation of a OH_b species in a nearby O_b site and the produced ·OH species desorbs from the reaction site [84]. Their results strongly support our assignment that the photocatalytic H_2O dissociation at Ti_{5c} site is dominated by the photo-generated holes.

The rate of photocatalytic dissociation of H_2O is quite low, which is mainly because the hole transfer is limited by the large energy difference between the redox potential of $H_2O/\cdot OH$ and valence band maximum (Fig.5(g)) [22]. CH_3OH is recognized as a typical hole scavenge in photocatalytic reactions [92–95], which can be another molecular system to detect the photocatalytic reaction on $TiO_2(110)$-(1×1) surface.

The adsorption behavior of CH_3OH on $TiO_2(110)$-(1×1) surface at 80 K is quite similar to H_2O. Figure 6 (a) and (b) show the images before and after CH_3OH dosing. It is observed the CH_3OH dominantly (~92%) adsorb at Ti_{5c} sites, presenting as bright spots at 80 K (Fig.6(b)). Similar to water at O_V sites, CH_3OH adsorbed at O_V sites could spontaneously dissociate to a CH_3O-OH_b pair at elevated temperatures [96] or under repeated scanning with the STM tip, as shown in Fig.6 (c) and (d).

Figure 6(e) shows seven adsorbed CH_3OH at the Ti_{5c} sites [27], and after 15 min 400 nm UV illumination, four CH_3OH molecules changed to an expanded feature, as marked by the white arrows in Fig.6(f). The expanded species can be attributed to a dissociative form of CH_3OH after UV light irradiation. To identify the reaction products, we manipulated one of expanded species along the direction labeled by "m1" in Fig.6(f). After the manipulation, the expanded species was separated to two parts (Fig.6(g)). Considering the possible reaction processes, we attributed these two parts to an OH_b and a CH_3O. More than 20 expanded species were manipulated, and quite repeated results were obtained. We therefore conclude that the reaction of CH_3OH under UV light irradiation undergoes O−H bond cleavage, and the H atom transfers to the nearby O_{br}, as illustrated in Fig.6(h). It is also found only the light with wavelength shorter than 400 nm could induce the reaction of CH_3OH. The efficiency of photocatalytic dissociation of CH_3OH was obvious higher than H_2O. Generally, ~18% CH_3OH molecules can be dissociated by a 5 min 266 nm UV irradiation with the nominal intensity of 1.0 mW/cm^2. The apparent quantum yield (AQY) is estimated from the number of dissociated molecules over by the number of incident photons per unit area [97]. With the low adsorption coverage of 0.02 ML and the light intensity of 1.0 mW/cm^2, the AQY is about $\sim 1\times10^{-7}$ and $\sim 1\times10^{-5}$ in our experiments for H_2O and CH_3OH dissociation respectively, showing the AQY of H_2O is smaller than that of CH_3OH by two orders of magnitude.

IV. IDENTIFICATION OF POINT DEFECTS ON ANATASE $TiO_2(001)$-(1×4) SURFACE

Anatase is another widely studied crystalline phase of TiO_2, which is suggested to be more catalytically

DOI:10.1063/1674-0068/28/cjcp1506129

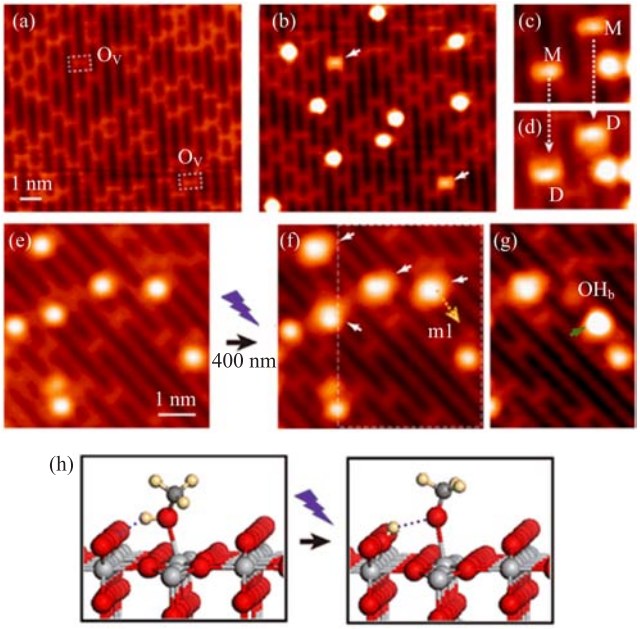

FIG. 6 (a) and (b) Same area STM images before and after CH_3OH dosing to the TiO_2(110)-(1×1) surface. Imaged at 1.0 V, 10 pA, 80 K. (c) and (d) Sequential STM images of CH_3OH dissociation at O_V. M: the molecular state CH_3OH at O_V, D: the dissociated CH_3O-OH_b pair with a tail at one side. (e) STM image of CH_3OH molecules at TiO_2(110)-(1×1) surface. (f) STM image of the same area after 15 min 400 nm light irradiation. White arrows mark the changed molecules with stretched feature. (g) After a later manipulation under the condition of 0.4 V and 700 pA in the orientation marked by "m1" in (f). The green arrow marks the separated CH_3O species. (h) Structure models of photocatalytic dissociation of CH_3OH at a Ti_{5c} site. (e)−(h) Modified with permission from Ref.[27], copyright 2010 The Royal Society of Chemistry.

active than rutile [8, 19, 98, 99]. For instance, Xu *et al.* reported in CO photo-oxidation, anatase (101) surface showed a substantially higher activity by an order of magnitude than the rutile (110) surface [100]. Theoretical calculations suggest the (001) surface has the highest reactivity and a lot of experimental efforts have been made to fabricate the (001) surface of single crystal anatase TiO_2 [15, 19, 98, 101]. However, the reactivity of the (001) surface is argued in recent experimental observations [102, 103], for example Pan *et al.* suggested the clean (001) exhibited lower reactivity than (101) in photooxidation reactions [102]. The direct atomistic level experiments to identify the active sites and even the surface structure of anatase TiO_2(001) are still limited [18, 104, 105]. One of the difficulties is the growth of a large size high quality anatase single crystal. To obtain a large size single crystal surface for STM experiments, the epitaxial growth of anatase film at the $SrTiO_3$(001) substrate has been studied by the methods of chemical vapor deposition [106], oxygen-plasma assisted molecular beam epitaxy [107], and pulse laser deposition (PLD) [108–110].

In our study, the high quality anatase TiO_2 films are epitaxially grown on the Nb-doped $SrTiO_3$ (0.7wt%) substrate by the PLD method [30, 111]. The TiO_2 film is grown at a very slow speed of ∼10 nm/h which is estimated from the period of RHEED intensity fluctuation. The typical thickness of film is about 30 nm to 60 nm. During TiO_2 deposition, the optimized O_2 pressure is 1.5×10^{-3} Pa and the substrate temperature is in the range of 773 K to 1023 K. Although such substrate temperature is already higher than the anatase-rutile phase transition temperature [11], the lattice matching [112] prevents the phase transition, leading to the TiO_2 thin film growing in anatase phase. The X-ray diffraction pattern obtained at the as-grown film in Fig.7 (a) and (b) shows a clear anatase (004) peak at ∼37.8°, which confirms that the films are in anatase phase and exhibiting a well-oriented (001) surface.

Figure 7(c) shows a typical large-scale STM image of the as-grown anatase TiO_2(001) surface. It is observed the surface consists of orthogonal ridges along the [100] and [010] directions. The ridge spacing is about 1.5 nm, which is about 4 times of the anatase lattice constant a (a=0.3786 nm). The atomic resolved STM image in the inset of Fig.7(c) shows the surface is of (1×4) reconstruction. Many dark spots can be observed at the ridge and imaged as individual point defects in the high resolution image as marked by white ellipses. Similar dark spots were also observed in previous studies [18, 104]. It was reported that Sr atoms might migrate from the $SrTiO_3$ substrate to the surface when TiO_2(001) films were grown at relatively high substrate temperatures [99, 108, 113]. By using XPS to monitor the Sr $3d_{5/2}$ core-level of different samples, we find the Sr contents will gradually increase as the substrate temperature increasing. However, the concentration of the dark spots in STM images decreases as the substrate temperature increasing. Our results suggest the dark spots at the ridges should be intrinsic point defects on anatase TiO_2(001)-(1×4) surface, but not the Sr impurities. The XPS spectra obtained at the as-grown anatase TiO_2 surface shows that the Ti 2p peaks locate at 458.7 eV ($2p_{3/2}$) and 464.4 eV ($2p_{1/2}$), as shown Fig.7(d), which correspond to the binding energies of the Ti^{4+} oxidation state [114, 115], suggesting the as-grown sample is almost fully oxidized. This should be attributed to the growth of the thin films under an O_2 condition.

The oxidized as-grown surface is further reduced by cycles of 2 keV Ar^+ ion sputtering for 4 min and UHV annealing at 873 K for 20 min. Figure 7(e) shows the STM image of the reduced anatase TiO_2(001)-(1×4) surface. It is observed that a large number of bright spots appear at the ridges in addition to the dark spot as compared with the as-grown surface. The inset of Fig.7(e) shows the high resolution image of the reduced surface, in which the bright spot defects are marked by red ellipses. Similar to the reduced rutile TiO_2, the

DOI:10.1063/1674-0068/28/cjcp1506129

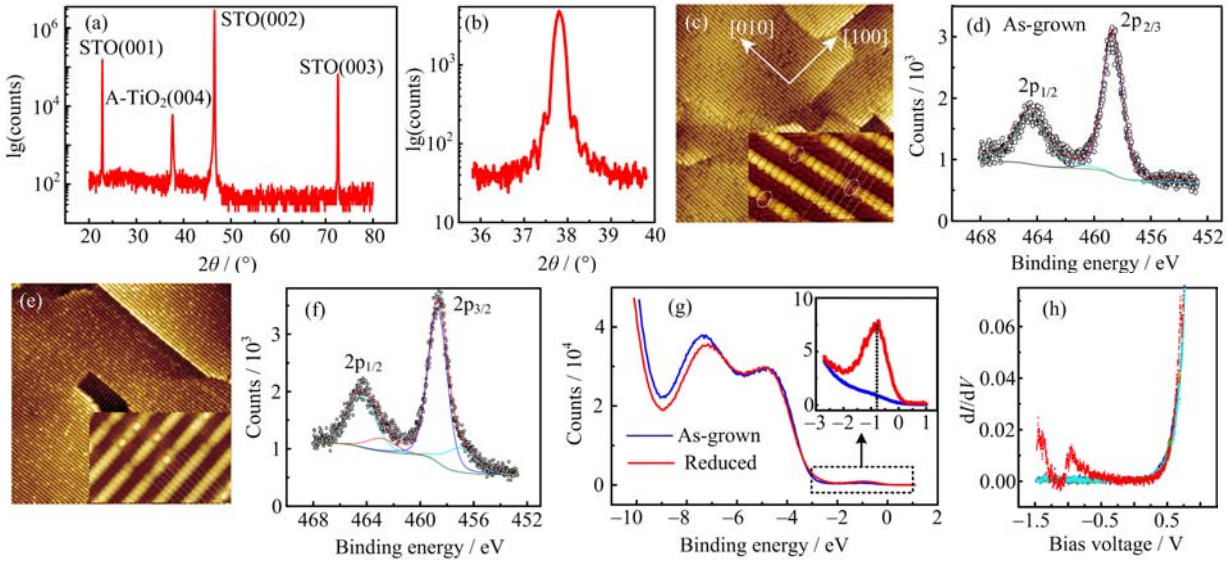

FIG. 7 (a) XRD pattern of the epitaxially grown anatase TiO_2(001) thin film (60 nm thick) on $SrTiO_3$(001) substrate. A-TiO_2 denotes anatase TiO_2, and STO denotes $SrTiO_3$. (b) High resolution XRD pattern at anatase TiO_2(004) peak. (c) STM image of the as-grown anatase TiO_2(001)-(1×4) surface. Inset is the high resolution image. (d) The XPS spectra for Ti 2p of the as-grown surface. (e) STM image of the reduced anatase TiO_2(001)-(1×4) surface. Inset is the high resolution image. Red ellipses mark the bright spot defects. (f) XPS spectra for Ti 2p of the reduced surface. (g) UPS spectra of the as-grown (blue) and the reduced (red) surface. (h) dI/dV curves recorded at a bright spot (red), a dark spot (blue), a normal ridge site (purple) and a terrace site (cyan), acquired at bias of 1.0 V and setpoint current of 100 pA. The three curves in blue, purple and cyan almost completely overlap. All data were measured at room temperature. Modified with permission from Ref.[30], Copyright 2013 Macmillan Publishers Limited.

Ti^{3+} signals raise at the reduced anatase surface in addition to Ti^{4+} signals, exhibiting two shoulder peaks of Ti^{3+} oxidation state at 457.1 and 463.1 eV in XPS spectra [116], as shown in Fig.7(f). The Ti^{3+} component is estimated to be ∼10%, showing the anatase TiO_2(001)-(1×4) surface is partially reduced. We further compared the band structures of as-grown and reduced surfaces by UPS spectra (Fig.7(g)). A defect state at −0.8 eV below Fermi level is only observed at the reduced surface, which can be assigned to the Ti^{3+} state. We also measured the dI/dV curves by STM at dark defects, bright defects, ridge sites and terrace sites. We found only the curve obtained at the bright spot presents a distinctive electronic state at −0.9 eV (Fig.7(h)). This electronic state at bright spot is in good agreement with the defect state measured by UPS, suggesting the bright spots should be responsible for the Ti^{3+} state on the reduced surface.

It is noted in previous studies, the 'ad-molecule' (ADM) model with fourfold-coordinated Ti was proposed for the reconstructed anatase TiO_2(001)-(1×4) surface [101, 117]. However, from our XPS results, only Ti^{4+} signal is observed at the as-grown surface, suggesting a fully oxidized surface. Considering the growth of thin films under O_2 atmosphere, we propose a model of sixfold-coordinated terminal Ti by modifying the ADM model, where an oxygen adatom is introduced in each unit cell, as shown by the optimized structural model in Fig.8(a). An asymmetric configuration of the ad-oxygen atoms is obtained from the DFT calculations. However, by considering the hopping of the ad-oxygen atom among the four equivalent sites (Fig.8(b)), the symmetric feature can be obtained in the simulated images (Fig.8(c)), in consistent with the symmetric oval appearance in the high resolution STM image (Fig.7(c)).

To understand the structures of the dark and bright spot defects on anatase TiO_2(001)-(1×4) surface, we use the STM tip to manipulate these defects. It is found the bright spots can be changed by applying pulses with voltage higher than 2.7 V. Three different processes are observed in the manipulations of bright spots, as shown in Fig.8 (d)−(f): (i) the bright spot changes to a dark spot (Fig.8(d)), (ii) the bright spot changes to a dark spot, accompanying with the appearance of a pair of fuzzy spots at the ridge nearby (Fig.8(e)), (iii) the bright spot changes to a "shouldered" dark spot with slightly protrusions at two sides (Fig.8(f)). Except the process I, the latter two can also be directly reversed by STM manipulation. Figure 8(h) shows the produced dark spot and a pair of fuzzy spots are converted back to a bright spot. Figure 8(i) shows "shouldered" dark spot is converted back to a bright spot by 2.7 V point pulses. The bright and the dark spots can also be directly interconverted (Fig.8(g)), which suggests that the dark and bright spots should have the same base structure. These behaviors under manipulation are highly reproducible.

Based on these facts, we propose that the dark spot

DOI:10.1063/1674-0068/28/cjcp1506129

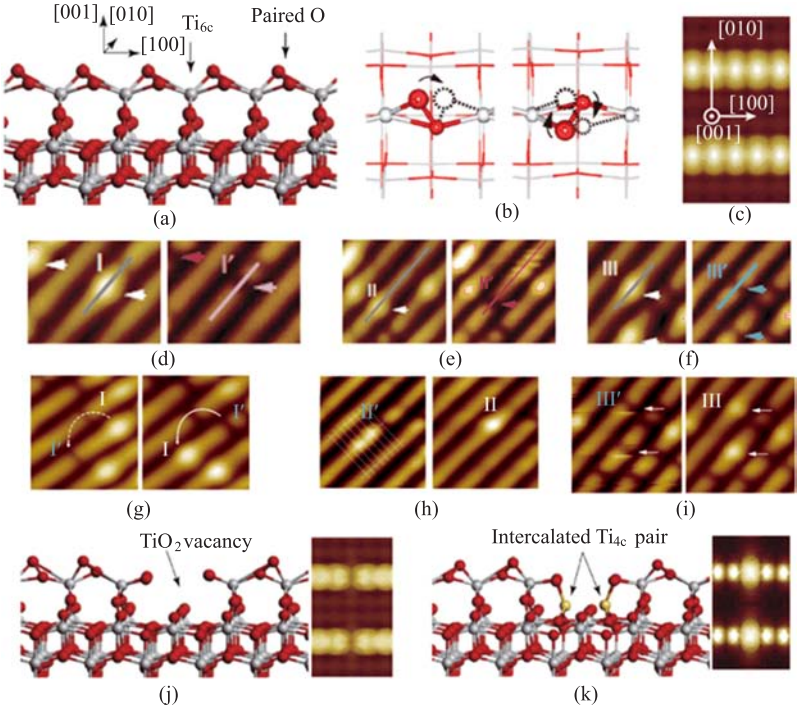

FIG. 8 (a) Optimized oxidized structural model of a perfect anatase TiO_2(001)-(1×4) surface. (b) Top view of the models showing the equivalent positions for the ad-oxygen atoms. (c) Simulated STM image of the perfect anatase TiO_2(001)-(1×4) surface. (d)−(f) Same area images show the changes of the bright spot (white arrows) by the voltage pulse of 3.7 V. (g) Images showing the direct conversion of a bright spot to a dark spot, manipulated by a 3.7 V pulse. (h) Images showing the reverse process (from II′ to II) manipulated by a 2.7 V pulse. (i) Images showing the reverse process (from III′ to III) manipulated by a 2.7 V pulse. All the images are obtained at 2.0 V and 10 pA. (j) The structural model and simulated image of a dark spot. (k) The structural model and simulated image of a bright spot. Figures are modified with permission from Ref.[30], copyright 2013 Macmillan Publishers Limited.

is a "TiO_2" vacancy at the ridge (Fig.8(j)), and the bright spot is formed by two intercalated Ti atoms into the TiO_2 vacancy (Fig.8(k)). The simulated images of the dark and bright spots according to these structural models are in good agreement with the experimental observations. In the model for the dark spot defects, the existence of TiO_2 vacancies does not change the ratio of Ti to O, so that the surface is still fully oxidized. However, in the case of the intercalated Ti atoms, the fourfold coordinated Ti atoms introduce Ti^{3+} state at the bright spot defects. These structural models can well explain the manipulation processes and qualitatively explain the electronic properties of the defects.

V. ADSORPTION BEHAVIORS OF H_2O AND O_2 ON ANATASE TiO_2(001)-(1×4) SURFACE

Adsorption and reaction of H_2O on anatase TiO_2(001)-(1×4) surface are widely concerned, and it is theoretically suggested that the anatase surface has superior reactivity for the spontaneous dissociation of H_2O [17, 101, 118].

We conducted *in situ* STM studies at 80 K to investigate the adsorption behaviors of H_2O at both as-grown and reduced anatase TiO_2(001)-(1×4) surface. At the oxidized surface, we do not observe any H_2O adsorption at low coverage. But at the reduced surface, we find the H_2O molecules can adsorb at the bright-spot defects. Figure 9(a) shows an area of the reduced surface with four bright spots and two dark spots. After 0.1 Langmuir H_2O dosing *in situ*, all the bright spots changed to dim spots, which behave a slightly different appearance as the native dark spots as shown in Fig.9(b). Such dim spots indicate H_2O adsorption at corresponding sites of the bright spot defects. After scanning at a relative higher bias voltage of 2.0 V, three of the dim spots changed to paired weak protrusions (Fig.9(c)), suggesting a reaction should have taken place. These phenomena are interpreted with the structural models as shown in Fig.9 (d) and (e). The dim spot is a singly adsorbed H_2O at the bright-spot defect (Fig.9(d)), which has an adsorption energy of 0.96 eV from the DFT calculations. The paired weak protrusions are assigned to the OH pair from the dissociated H_2O (Fig.9(e)). Our results indicate that the H_2O cannot spontaneously dissociate even at the bright-spot defect at 80 K. The tip induced H_2O dissociation at bright-spot defect might follow the same mechanisms of O_2 and H_2O dissociation at the defect of oxygen vacancy on rutile TiO_2(110) surface,

DOI:10.1063/1674-0068/28/cjcp1506129

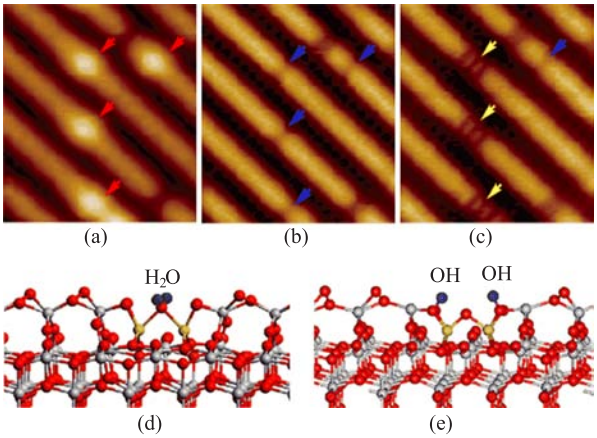

FIG. 9 (a)−(c) STM images of the reduced anatase TiO_2(001)-(1×4) surface (imaged at 1.5 V and 10 pA) within the same area acquired before H_2O dosing, after 0.1 Langmuir H_2O dosing *in situ*, and after scanning at 2.0 V and 10 pA, respectively. (d) and (e) Structure models of molecular H_2O and dissociated H_2O at the bright spot defect. Modified with permission from Ref.[30], copyright 2013 Macmillan Publishers Limited.

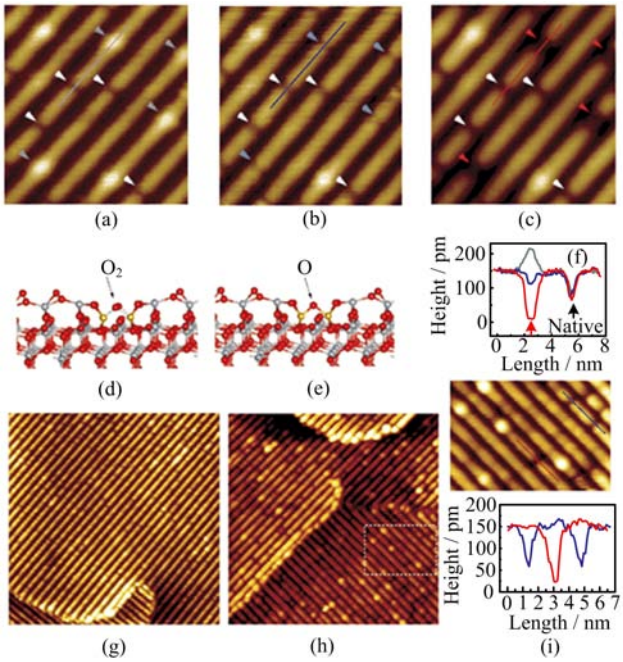

FIG. 10 (a)−(c) STM images of the reduced anatase TiO_2(001)-(1×4) surface (imaged at 1.5 V and 10 pA) within the same area acquired before and after 0.1 Langmuir O_2 dosing *in situ*. (c) Structure models of molecular O_2 at the bright spot defect. (d) The same area STM image obtained after scanning at 2.2 V. (e) Structure models of dissociated O_2 at the bright spot defect. (f) Line profiles along the marked positions in (a), (b), (d). The black arrow marks a native dark spot and the red arrow show the changes of a bright spot with O_2 adsorption and dissociation. (g) and (h) STM images of the reduced anatase TiO_2(001)-(1×4) surface obtained after 2 Langmuir O_2 dosing at room temperature, and after further annealing at 360 K for 20 min. (i) Magnified image of the marked rectangle in (h) and line profiles showing two typical depths of the dark spots after annealing. (Modified with permission from Ref.[30], copyright 2013 Macmillan Publishers Limited).

as discussed above. With a large amount of 2 Langmuir H_2O dosing, fuzzy STM images are observed and the ridges cannot be imaged clearly, which indicates the adsorption of H_2O at the ridge site is fairly unstable at 80 K. This is consistent to the low adsorption energy of 0.45 eV for H_2O at ridge site. At room temperature, we did not observe any obvious adsorption behavior for H_2O at both as-grown and reduced surfaces.

Adsorption behavior of O_2 on anatase TiO_2(001)-(1×4) surface is quite similar to H_2O. Only the bright-spot defects at the reduced surface are the active sites for O_2 adsorption. Figure 10 (a) and (b) are the images within the same area before and after 0.1 Langmuir O_2 dosing at 80 K. It is observed four bright spots marked by red arrows changed to dim spots, indicating O_2 adsorption at the bright spot defects. The optimized structure shows O_2 is bonding to the two intercalated Ti atoms, with a large adsorption energy of 1.80 eV (Fig.10(c)). After a 2.2 V voltage scanning, the dim spots with O_2 adsorption changed to much darker spots because of the dissociation of O_2 at the defect, as shown in Fig.10 (d) and (e). The line profiles in Fig.10(f) at the corresponding positions clearly show the changes of these species.

At room temperature, it is found that O_2 can still stably adsorbed at the bright-spot defects on reduced TiO_2(001)-(1×4) surface. Figure 10(g) was obtained after 2 Langmuir O_2 dosing. It is observed nearly all the bright spots disappear at the surface. Furthermore, the O_2 adsorbed surface was annealed to 360 K. After annealing for 20 min, it is found that some of the bright spots reappear (Fig.10 (h) and (i)). In addition to the native dark spots, the much darker spots can be attributed to the dissociative O_2, similar to the observations at 80 K. These results suggest molecular O_2 can adsorb at the bright-spot defects at room temperature. Upon heating to 360 K, some of the adsorbed O_2 may desorb from the bright spot defects, and some of them may dissociate at the bright-spot defects. When the surface was further annealing at the elevated temperature higher than 500 K, statistically, the concentration of the bright spots was recovered, indicating almost all of the adsorbed O_2 had desorbed from the surface.

VI. CONCLUSION AND PROSPECTS

By using STM, we have provided an atomistic view of the reactivity of rutile TiO_2(110)-(1×1) surface and anatase TiO_2(001)-(1×4) surface. The adsorption and reaction behaviors of several molecules, such as O_2, CO_2, H_2O and CH_3OH, have been characterized at

DOI:10.1063/1674-0068/28/cjcp1506129

both of rutile TiO_2(110)-(1×1) surface and anatase TiO_2(001)-(1×4) surface. At rutile TiO_2(110)-(1×1) surface, the O_V defects serve as the prior active sites for O_2 and CO_2 adsorption and dissociation. Also, the terminal Ti_{5c} sites are found to be the active sites for the photocatalytic reaction of H_2O and CH_3OH. The initial reaction steps of photo-oxidation of H_2O and CH_3OH by the photo generated holes have been directly observed. At the anatase TiO_2(001)-(1×4) surface, the Ti-rich point defects, which introduce the Ti^{3+} defect state to the surface, show distinct reactivity in the adsorption and reaction of O_2 and H_2O.

By comparing the reactions of O_2 and H_2O at rutile TiO_2(110)-(1×1) surface and anatase TiO_2(001)-(1×4) surface at the similar experimental conditions, we do not observe any priority for the anatase (001) surface. This is largely different from the conventional knowledge that the anatase, especially the (001) surface is the most reactive. Our findings about the active sites and molecules level chemical reactions can provide useful information for the understanding of the mechanisms of the TiO_2 catalysis and also for the synthesis of higher reactivity TiO_2 surfaces.

VII. ACKNOWLEDGMENTS

This work was supported by the Ministry of Science and Technology of China (No.2011CB921400), the "Strategic Priority Research Program" of the Chinese Academy of Sciences (No.XDB01020100), and the National Natural Science Foundation of China.

[1] A. Fujishima and K. Honda, Nature **238**, 37 (1972).
[2] M. A. Henderson and I. Lyubinetsky, Chem. Rev. **113**, 4428 (2013).
[3] C. L. Pang, R. Lindsay, and G. Thornton, Chem. Soc. Rev. **37**, 2328 (2008).
[4] Z. Dohnálek, I. Lyubinetsky, and R. Rousseau, Prog. Surf. Sci. **85**, 161 (2010).
[5] P. Salvador, Prog. Surf. Sci. **86**, 41 (2011).
[6] U. Diebold, Surf. Sci. Rep. **48**, 53 (2003).
[7] A. Fujishima, X. T. Zhang, and D. A. Tryk, Surf. Sci. Rep. **63**, 515 (2008).
[8] M. A. Henderson, Surf. Sci. Rep. **66**, 185 (2011).
[9] A. L. Linsebigler, G. Q. Lu, and J. T. Yates, Chem. Rev. **95**, 735 (1995).
[10] J. T. Yates, Surf. Sci. **603**, 1605 (2009).
[11] D. A. H. Hanaor and C. C. Sorrell, J. Mater. Sci. **46**, 855 (2011).
[12] A. Imanishi, T. Okamura, N. Ohashi, R. Nakamura, and Y. Nakato, J. Am. Chem. Soc. **129**, 11569 (2007).
[13] R. Nakamura, T. Okamura, N. Ohashi, A. Imanishi, and Y. Nakato, J. Am. Chem. Soc. **127**, 12975 (2005).
[14] Á Valdés, Z. W. Qu, G. J. Kroes, J. Rossmeisl, and J. K. Norskov, J. Phys. Chem. C **112**, 9872 (2008).
[15] H. G. Yang, C. H. Sun, S. Z. Qiao, J. Zou, G. Liu, S. C. Smith, H. M. Cheng, and G. Q. Lu, Nature **453**, 638 (2008).
[16] Y. B. He, A. Tilocca, O. Dulub, A. Selloni, and U. Diebold, Nat. Mater. **8**, 585 (2009).
[17] X. Q. Gong and A. Selloni, J. Phys. Chem. B **109**, 19560 (2005).
[18] F. Silly and M. R. Castell, Appl. Phys. Lett. **85**, 3223 (2004).
[19] A. Vittadini, A. Selloni, F. P. Rotzinger, and M. Grätzel, Phys. Rev. Lett. **81**, 2954 (1998).
[20] X. F. Cui, B. Wang, Z. Wang, T. Huang, Y. Zhao, J. L. Yang, and J. G. Hou, J. Chem. Phys. **129**, 044703 (2008).
[21] X. F. Cui, Z. Wang, S. J. Tan, B. Wang, J. L. Yang, and J. G. Hou, J. Phys. Chem. C **113**, 13204 (2009).
[22] S. J. Tan, H. Feng, Y. F. Ji, Y. Wang, J. Zhao, A. D. Zhao, B. Wang, Y. Luo, J. L. Yang, and J. G. Hou, J. Am. Chem. Soc. **134**, 9978 (2012).
[23] S. J. Tan, Y. Zhao, J. Zhao, Z. Wang, C. X. Ma, A. D. Zhao, B. Wang, Y. Luo, J. L. Yang, and J. G. Hou, Phys. Rev. B **84**, 155418 (2011).
[24] S. J. Tan, Y. F. Ji, Y. Zhao, A. D. Zhao, B. Wang, J. L. Yang, and J. G. Hou, J. Am. Chem. Soc. **133**, 2002 (2011).
[25] Z. Wang, Y. Zhao, X. F. Cui, S. J. Tan, A. D. Zhao, B. Wang, J. L. Yang, and J. G. Hou, J. Phys. Chem. C **114**, 18222 (2010).
[26] Y. Zhao, Z. Wang, X. F. Cui, T. Huang, B. Wang, Y. Luo, J. L. Yang, and J. G. Hou, J. Am. Chem. Soc. **131**, 7958 (2009).
[27] C. Y. Zhou, Z. F. Ren, S. J. Tan, Z. B. Ma, X. C. Mao, D. X. Dai, H. J. Fan, and X. M. Yang, J. LaRue, R. Cooper, A. M. Wodtke, Z. Wang, Z. Y. Li, B. Wang, J. L. Yang, and J. G. Hou, Chem. Sci. **1**, 575 (2010).
[28] Y. Ji, B. Wang, and Y. Luo, J. Phys. Chem. C **116**, 7863 (2012).
[29] Y. Ji, B. Wang, and Y. Luo, J. Phys. Chem. C **117**, 956 (2012).
[30] Y. Wang, H. J. Sun, S. J. Tan, H. Feng, Z. W. Cheng, J. Zhao, A. D. Zhao, B. Wang, Y. Luo, J. L. Yang, and J. G. Hou, Nat. Commun. **4**, 2214 (2013).
[31] N. Shibata, A. Goto, S. Y. Choi, T. Mizoguchi, S. D. Findlay, T. Yamamoto, and Y. Ikuhara, Science **322**, 570 (2008).
[32] S. Wendt, P. T. Sprunger, E. Lira, G. K. H. Madsen, Z. S. Li, J. Ø. Hansen, J. Matthiesen, A. Blekinge-Rasmussen, E. Lægsgaard, B. Hammer, and F. Besenbacher, Science **320**, 1755 (2008).
[33] R. Schaub, R. Thostrup, N. Lopez, E. Lægsgaard, I. Stensgaard, J. K. Norskov, and F. Besenbacher, Phys. Rev. Lett. **87**, 266104 (2001).
[34] Z. Zhang, Q. Ge, S. C. Li, B. D. Kay, J. M. White, and Z. Dohnálek, Phys. Rev. Lett. **99**, 126105 (2007).
[35] C. M. Yim, C. L. Pang, and G. Thornton, Phys. Rev. Lett. **104**, 036806 (2010).
[36] T. Minato, Y. Sainoo, Y. Kim, H. S. Kato, K. Aika, M. Kawai, J. Zhao, H. Petek, T. Huang, W. He, B. Wang, Z. Wang, Y. Zhao, J. L. Yang, and J. G. Hou, J. Chem. Phys. **130**, 124502 (2009).
[37] V. E. Henrich, G. Dresselhaus, and H. J. Zeiger, Phys. Rev. Lett. **36**, 1335 (1976).
[38] M. A. Henderson, W. S. Epling, C. H. F. Peden, and

DOI:10.1063/1674-0068/28/cjcp1506129

C. L. Perkins, J. Phys. Chem. B **107**, 534 (2003).
[39] C. Di Valentin, G. Pacchioni, and A. Selloni, Phys. Rev. Lett. **97**, 166803 (2006).
[40] Z. Zhang, K. Cao, and J. T. Yates, J. Phys. Chem. Lett. **4**, 674 (2013).
[41] M. Batzill, K. Katsiev, D. J. Gaspar, and U. Diebold, Phys. Rev. B **66**, 235401 (2002).
[42] N. A. Deskins, R. Rousseau, and M. Dupuis, J. Phys. Chem. C **114**, 5891 (2010).
[43] A. C. Papageorgiou, N. S. Beglitis, C. L. Pang, G. Teobaldi, G. Cabailh, Q. Chen, A. J. Fisher, W. A. Hofer, and G. Thornton, Proc. Natl. Acad. Sci. USA **107**, 2391 (2010).
[44] K. Mitsuhara, H. Okumura, A. Visikovskiy, M. Takizawa, and Y. Kido, J. Chem. Phys. **136**, 124707 (2012).
[45] T. Berger, M. Sterrer, O. Diwald, and E. Knozinger, ChemPhysChem **6**, 2104 (2005).
[46] S. Chrétien and H. Metiu, J. Chem. Phys. **129**, 074705 (2008).
[47] G. A. Kimmel and N. G. Petrik, Phys. Rev. Lett. **100**, 196102 (2008).
[48] E. Lira, J. Ø. Hansen, P. Huo, R. Bechstein, P. Galliker, E. Lægsgaard, B. Hammer, S. Wendt, and F. Besenbacher, Surf. Sci. **604**, 1945 (2010).
[49] N. G. Petrik and G. A. Kimmel, J. Phys. Chem. Lett. **1**, 1758 (2010).
[50] N. G. Petrik, Z. R. Zhang, Y. G. Du, Z. Dohnalek, I. Lyubinetsky, and G. A. Kimmel, J. Phys. Chem. C **113**, 12407 (2009).
[51] D. Pillay, Y. Wang, and G. S. Hwang, J. Am. Chem. Soc. **128**, 14000 (2006).
[52] M. D. Rasmussen, L. M. Molina, and B. Hammer, J. Chem. Phys. **120**, 988 (2004).
[53] A. Tilocca and A. Selloni, ChemPhysChem **6**, 1911 (2005).
[54] Y. Wang, D. Pillay, and G. S. Hwang, Phys. Rev. B **70**, 193410 (2004).
[55] Z. T. Wang, N. Aaron Deskins, and I. Lyubinetsky, J. Phys. Chem. Lett. **3**, 102 (2011).
[56] S. Wendt, R. Schaub, J. Matthiesen, E. K. Vestergaard, E. Wahlstrom, M. D. Rasmussen, P. Thostrup, L. M. Molina, E. Lægsgaard, I. Stensgaard, B. Hammer, and F. Besenbacher, Surf. Sci. **598**, 226 (2005).
[57] M. A. Henderson, W. S. Epling, C. L. Perkins, C. H. F. Peden, and U. Diebold, J. Phys. Chem. B **103**, 5328 (1999).
[58] P. Scheiber, Riss A., M. Schmid, P. Varga, and U. Diebold, Phys. Rev. Lett. **105**, 216101 (2010).
[59] Z. T. Wang, Y. Du, Z. Dohnálek, and I. Lyubinetsky, J. Phys. Chem. Lett. **1**, 3524 (2010).
[60] Y. G. Du, N. A. Deskins, Z. R. Zhang, Z. Dohnálek, M. Dupuis, and I. Lyubinetsky, Phys. Chem. Chem. Phys. **12**, 6337 (2010).
[61] N. G. Petrik and G. A. Kimmel, J. Phys. Chem. Lett. **4**, 344 (2013).
[62] J. C. Hemminger, R. Carr, and G. A. Somorjai, Chem. Phys. Lett. **57**, 100 (1978).
[63] T. Sakakura, J. C. Choi, and H. Yasuda, Chem. Rev. **107**, 2365 (2007).
[64] C. S. Song, Catal. Today **115**, 2 (2006).
[65] H. Arakawa, M. Aresta, J. N. Armor, M. A. Barteau, E. J. Beckman, A. T. Bell, J. E. Bercaw, C. Creutz, E. Dinjus, D. A. Dixon, K. Domen, D. L. DuBois, J. Eckert, E. Fujita, D. H. Gibson, W. A. Goddard, D. W. Goodman, J. Keller, G. J. Kubas, H. H. Kung, J. E. Lyons, L. E. Manzer, T. J. Marks, K. Morokuma, K. M. Nicholas, R. Periana, L. Que, J. Rostrup-Nielson, W. M. H. Sachtler, L. D. Schmidt, A. Sen, G. A. Somorjai, P. C. Stair, B. R. Stults, and W. Tumas, Chem. Rev. **101**, 953 (2001).
[66] H. J. Freund and M. W. Roberts, Surf. Sci. Rep. **25**, 225 (1996).
[67] T. Inoue, A. Fujishima, S. Konishi, and K. Honda, Nature **277**, 637 (1979).
[68] N. S. Lewis and D. G. Nocera, Proc. Natl. Acad. Sci. USA **103**, 15729 (2006).
[69] S. C. Roy, O. K. Varghese, M. Paulose, and C. A. Grimes, Acs Nano **4**, 1259 (2010).
[70] V. P. Indrakanti, J. D. Kubicki, and H. H. Schobert, Energ. Environ. Sci. **2**, 745 (2009).
[71] D. P. Acharya, N. Camillone, and P. Sutter, J. Phys. Chem. C **115**, 12095 (2011).
[72] J. Lee, D. C. Sorescu, X. Deng, and K. D. Jordan, J. Phys. Chem. Lett. **2**, 3114 (2011).
[73] J. Lee, D. C. Sorescu, and X. Y. Deng, J. Am. Chem. Soc. **133**, 10066 (2011).
[74] X. Lin, Y. Yoon, N. G. Petrik, Z. J. Li, Z. T. Wang, V. A. Glezakou, B. D. Kay, I. Lyubinetsky, G. A. Kimmel, R. Rousseau, and Z. Dohnálek, J. Phys. Chem. C **116**, 26322 (2012).
[75] D. C. Sorescu, J. Lee, W. A. Al-Saidi, and K. D. Jordan, J. Chem. Phys. **134**, 104707 (2011).
[76] L. Gundlach, R. Ernstorfer, and F. Willig, Phys. Rev. B **74**, 035324 (2006).
[77] Á. Valdés and G. J. Kroes, J. Phys. Chem. C **114**, 1701 (2010).
[78] M. A. Henderson, Langmuir **12**, 5093 (1996).
[79] M. A. Henderson, Surf. Sci. **355**, 151 (1996).
[80] M. A. Henderson, Surf. Sci. **400**, 203 (1998).
[81] O. Bikondoa, C. L. Pang, R. Ithnin, C. A. Muryn, H. Onishi, and G. Thornton, Nat. Mater. **5**, 189 (2006).
[82] S. C. Li, Z. Zhang, D. Sheppard, B. D. Kay, J. M. White, Y. Du, I. Lyubinetsky, G. Henkelman, and Z. Dohnálek, J. Am. Chem. Soc. **130**, 9080 (2008).
[83] J. Matthiesen, J. Ø. Hansen, S. Wendt, E. Lira, R. Schaub, E. Lægsgaard, F. Besenbacher, and B. Hammer, Phys. Rev. Lett. **102**, 226101 (2009).
[84] J. Lee, D. C. Sorescu, X. Y. Deng, and K. D. Jordan, J. Phys. Chem. Lett. **4**, 53 (2013).
[85] S. Wendt, J. Matthiesen, R. Schaub, E. K. Vestergaard, E. Lægsgaard, F. Besenbacher, and B. Hammer, Phys. Rev. Lett. **96**, 066107 (2006).
[86] J. Oviedo, R. Sanchez-De-Armas, M. A. S. Miguel, and J. F. Sanz, J. Phys. Chem. C **112**, 17737 (2008).
[87] D. P. Acharya, C. V. Ciobanu, N. Camillone, and P. Sutter, J. Phys. Chem. C **114**, 21510 (2010).
[88] J. W. Tang, J. R. Durrant, and D. R. Klug, J. Am. Chem. Soc. **130**, 13885 (2008).
[89] Y. Ohko, K. Hashimoto, and A. Fujishima, J. Phys. Chem. A **101**, 8057 (1997).
[90] T. Yoshihara, R. Katoh, A. Furube, Y. Tamaki, M. Murai, K. Hara, S. Murata, H. Arakawa, and M. Tachiya, J. Phys. Chem. B **108**, 3817 (2004).
[91] A. Fujishima, T. N. Rao, and D. A. Tryk, J. Photochem. Photobio. C **1**, 1 (2000).

DOI:10.1063/1674-0068/28/cjcp1506129

[92] T. L. Thompson and J. T. Yates, J. Phys. Chem. B **109**, 18230 (2005).
[93] M. M. Shen and M. A. Henderson, J. Phys. Chem. Lett. **2**, 2707 (2011).
[94] J. Zhao, J. L. Yang, and H. Petek, Phys. Rev. B **80**, 235416 (2009).
[95] M. A. Henderson, S. Otero-Tapia, and M. E. Castro, Faraday Discuss. **114**, 313 (1999).
[96] Z. R. Zhang, O. Bondarchuk, J. M. White, B. D. Kay, and Z. Dohnálek, J. Am. Chem. Soc. **128**, 4198 (2006).
[97] A. Kudo and Y. Miseki, Chem. Soc. Rev. **38**, 253 (2009).
[98] A. Beltran, J. R. Sambrano, M. Calatayud, F. R. Sensato, and J. Andres, Surf. Sci. **490**, 116 (2001).
[99] G. S. Herman and Y. Gao, Thin Solid Films **397**, 157 (2001).
[100] M. C. Xu, Y. K. Gao, E. M. Moreno, M. Kunst, M. Muhler, Y. M. Wang, H. Idriss, and C. Woll, Phys. Rev. Lett. **106**, 138302 (2011).
[101] M. Lazzeri, A. Vittadini, and A. Selloni, Phys. Rev. B **63**, 155409 (2001).
[102] J. Pan, G. Liu, G. Q. Lu, and H. M. Cheng, Angew Chem. Int. Ed. **50**, 2133 (2011).
[103] T. Tachikawa, S. Yamashita, and T. Majima, J. Am. Chem. Soc. **133**, 7197 (2011).
[104] Y. Du, D. J. Kim, T. C. Kaspar, S. E. Chamberlin, I. Lyubinetsky, and S. A. Chambers, Surf. Sci. **606**, 1443 (2012).
[105] Y. Xia, K. Zhu, T. C. Kaspar, Y. Du, B. Birmingham, K. T. Park, and Z. Zhang, J. Phys. Chem. Lett. **4**, 2958 (2013).
[106] G. S. Herman, M. R. Sievers, and Y. Gao, Phys. Rev. Lett. **84**, 3354 (2000).
[107] Y. Liang, S. P. Gan, S. A. Chambers, and E. I. Altman, Phys. Rev. B **63**, 235402 (2001).
[108] T. Ohsawa, Y. Yamamoto, M. Sumiya, Y. Matsumoto, and H. Koinuma, Langmuir **20**, 3018 (2004).
[109] C. C. Hsieh, K. H. Wu, J. Y. Juang, T. M. Uen, J. Y. Lin, and Y. S. Gou, J. Appl. Phys. **92**, 2518 (2002).
[110] S. Yamamoto, T. Sumita, T. Yamaki, A. Miyashita, and H. Naramoto, J. Cryst. Growth **237**, 569 (2002)
[111] Y. Wang, Z. W. Cheng, S. J. Tan, X. Shao, B. Wang, and J. G. Hou, Surf. Sci. **616**, 93 (2013).
[112] R. J. Kennedy and P. A. Stampe, J. Cryst. Growth **252,** 333 (2003).
[113] T. Ohsawa, I. V. Lyubinetsky, M. A. Henderson, and S. A. Chambers, J. Phys. Chem. C **112**, 20050 (2008).
[114] S. C. Li and U. Diebold, J. Am. Chem. Soc. **132**, 64 (2010).
[115] N. Ruzycki, G. S. Herman, L. A. Boatner, and U. Diebold, Surf. Sci. **529**, L239 (2003).
[116] R. E. Tanner, Y. Liang, and E. I. Altman, Surf. Sci. **506**, 251 (2002).
[117] X. Q. Gong, A. Selloni, and A. Vittadini, J. Phys. Chem. B **110**, 2804 (2006).
[118] A. Vittadini, M. Casarin, and A. Selloni, Theor. Chem. Acc. **117**, 663 (2007).

DOI:10.1063/1674-0068/28/cjcp1506129